Description of Advanced Deformation Models for FRAP-6

V.N. Shah
Water Reactor Research Dept.
E.R. Carlson
FARAD Branch
G.A. Berna
FARAD Branch
EG and G Idaho, Inc., P.O. Box 1625, Idaho Falls, Idaho 83415, U.S.A.

Summary

This paper presents a description of the cladding axial elongation models developed at the Idaho National Engineering Laboratory (INEL) for use by the FRAP-T6 computer code in analyzing the response of fuel rods during reactor transients in light water reactors (LWR). The FRAP-T6 code contains models (FRACAS-II subcode) that analyze the structural response of a fuel rod including pellet-cladding-mechanical-interaction (PCMI). Recently, four models were incorporated into FRACAS-II to calculate cladding axial deformation: (a) axial PCMI, (b) trapped fuel stack, (c) fuel relocation, and (d) effective fuel thermal expansion.

FRACAS-II is based on small strain theory. It performs an axisymmetric analysis to evaluate the elastic-plastic-creep response of fuel and cladding. Fuel pellet ends are assumed to be flat and the generalized plane strain assumption is used. At each time step, the method of successive elastic solutions is used to obtain an elastic-plastic and creep solution for the stresses and strains in the cladding.

The axial PCMI model has the capability to start axial PCMI at lower rod power than is needed for radial PCMI. The axial PCMI starts at lower rod power than does radial PCMI because of several reasons: random pellet stacking, pellect cocking, cladding ovality, etc. When axial PCMI takes place, the lower portion of the pellet column is trapped between the bottom of the cladding tube and the lowest pellet experiencing PCMI. The trapped-stack model anlayzes the trapped pellet column and the corresponding cladding section. The fuel relocation model allows for the fuel void due to pellet cracking, which reduces the effective gap between pellet and cladding. This fuel "relocation" as a function of as-fabricated gap, power, and burnup is included in FRAP-T6. The effective fuel thermal expansion model accounts for pellet design parameters in calculating the axial thermal expansion of a fuel stack. The pellet design parameters include the length of pellet and shape of the pellet ends. The pellet ends may be flat or dished, and/or chamfered.

Comparisons of cladding axial elongation measurements from two experiments with the corresponding FRAP-T6 calculations are presented.

---

a. Work supported by the U.S. Nuclear Regulatory Commission, Office of Nuclear Regulatory Research under DOE Contract No. DE-AC07-76ID01570.

1. Introduction

An LWR fuel rod consists of UO_2 fuel pellets enclosed in zircaloy cladding. The most important function of the cladding is to contain the radioactive fission products within the fuel rod. If the cladding does not fail (crack, rupture, or melt) during a reactor operation, radioactive fission products are contained by the cladding and pose no health hazard. Irradiation of an LWR fuel to high burnups requires that the rod remain free of metallurgical, chemical, and mechanical problems that could lead to failure of the cladding.

One possible source of failure is the high cladding stresses caused by the mechanical interaction between pellet and cladding (PCMI). This interaction is likely because the UO_2 fuel pellets expand more than does the zircaloy cladding. The increased expansion is due to higher fuel temperature, greater thermal expansion coefficient, cracking, and swelling. Cladding stresses due to PCMI depend upon the as-fabricated gap between fuel and cladding, rod power, rate of power increase, fuel burnup, cladding properties, and pellet design parameters. Sufficiently high stresses may crack the cladding releasing the radioactive fission products. Therefore, an accurate analysis of stresses in the cladding during PCMI is required to evaluate the structural integrity of cladding.

The capability to accurately calculate the performance of LWR fuel rods during transient and hypothetical accident conditions is a major objective of the Nuclear Regulatory Commission's (NRC) Water Reactor Safety Program. To achieve this objective, NRC is sponsoring development of the FRAPCON-2 (Fuel Rod Analysis Program--Steady State) [1] and FRAP-T6 (Fuel Rod Analysis Program--Transient) [2] computer codes. FRAPCON-2 calculates the steady state response of an LWR fuel rod during long-term burnup. FRAP-T6 calculates the transient response of an LWR fuel rod during operational transients and hypothetical accidents. FRAPCON-2 and FRAP-T6 use the FRACAS-II mechanics model [3] to calculate elastic-plastic-creep deformation of cladding and fuel during PCMI. FRACAS-II assumes generalized plane strain in the fuel rod and uses the transfer matrix method to solve pseudoelastic equations at each iteration in the axisymmetric, incremental elastic-plastic-creep analysis of cladding and fuel.

An accurate calculation of cladding stresses is essential in determining cladding failure because of stress corrosion cracking (SCC). When UO_2 expands thermally, its interaction with the cladding is manifested through axial and diametral deformation of cladding. The resulting cladding stresses may be divided into three components: (a) uniform axial stress, (b) hoop stress, and (c) localized axial stress because of ridge formation. The uniform axial stress in cladding is due to cladding elongation caused by the axial thermal expansion of fuel during PCMI. Recently, four models were added to FRACAS-II to calculate the cladding elongation during PCMI. This paper presents the description and assessment of these models.

The cladding elongation models are described in Section 2. Section 3 presents a comparison of experimental measurements of cladding axial extensions with corresponding FRAP-T6 calculations. Section 4 presents conclusions.

2. Model Description

Four models required to calculate the axial deformation in cladding during PCMI are described in this section. The first two models are mechanistically based while the remaining models are based on empirical relations. The axial PCMI model is described first. The trapped-stack model is described next. Then, the fuel relocation model and effective fuel thermal expansion models are described.

2.1 Axial PCMI Model

The axial PCMI model initiates an axial PCMI at lower power than is needed for radial PCMI. Axial PCMI requires only a few contact points to establish firm axial contact between cladding and pellet, while radial PCMI requires contact between cladding and pellet around the complete circumference. Axial PCMI starts at lower rod power than radial PCMI for any of several reasons: random pellet stacking, pellet cocking, cladding ovality, cladding eccentricity, pellet chipping, grid spacer pinching of cladding, and/or pellet hourglassing. A simple model is developed to address this phenomena. This model initiates axial PCMI earlier than the radial PCMI during increasing power and ceases axial and radial PCMI simultaneously during decreasing power. This model assumes that axial PCMI begins when the radial gap between cladding and fuel is less than the locking gap [4]. Based on measurements of cladding hoop and axial strains during a power cycle, an empirical model for locking gap can be developed.

The magnitude of the locking gap is largest during the first power cycle and reduces to zero during subsequent power cycles. Initially the randomly stacked pellets are in partial contact with the cladding tube at several points along the fuel rod. During the first power ramp, most of the original eccentricity is removed. So, during subsequent power cycles, the magnitude of the locking gap reduces to zero. Ultimately, axial and radial PCMI will begin at approximately the same power [5].

One of the following three configurations may be present during FRACAS-II analysis: open gap, axial PCMI, or radial PCMI. For the open gap configuration, there is no coupling between pellet and cladding. For axial PCMI, there is only axial coupling between pellet and cladding. For radial PCMI, there is radial and axial coupling between pellet and cladding. For all three configurations, the generalized plane strain equation along the axial direction is satisfied to determine the axial stresses. All three configurations are analyzed by the transfer matrix method [6].

2.2 Trapped-Stack Model

The mechanical interaction between pellet and cladding causes the trapping of the lower portion of the pellet column between the bottom of the cladding tube and the lowest pellet experiencing PCMI. The existence of the trapped-stack configuration is due to the nonuniform axial power profile of the fuel rod. Generally, the axial power profile is of chopped cosine shape and has a peak somewhere near the middle of the rod as shown in Figure 1. The pellets near the peak of the axial power profile experience axial PCMI at a lower power than the other pellets and trap the stack of pellets in the lower portion of the rod. If the axial power profile is uniform, then all the pellets experience axial PCMI at approximately the same power and the trapped-stack configuration does not exist. In the development of the trapped-stack model, an idealized trapped-stack condition representing only one trapped stack in the lower portion of the fuel rod is assumed.

Once the stack of pellets is trapped between the bottom of the cladding tube and the lowest pellet experiencing axial PCMI, the trapped stack and the corresponding length of cladding tube will experience the same change in axial length. As the temperature and thermal expansion coefficient for the fuel are greater than that of the cladding, pellets in the trapped-fuel stack will experience compressive stress and the associated cladding will experience tensile stress. The constraint of equal change in the axial length of the trapped fuel stack and the corresponding cladding section is called the compatibility condition. The fuel and cladding have time independent and time dependent deformations. The time independent deformations include elastic deformation of pellet and elastic-plastic deformation of cladding. The time dependent deformation is due to fuel and cladding creep. The compatability conditions for elastic-plastic and creep deformations are satisfied and the tensile stresses in the cladding length associated with the trapped fuel stack are calculated by the method of successive elastic solutions [7]. The details of this solution procedure are given in References 6 and 8.

As reactor power is increased from zero, first axial PCMI takes place at an elevation near the peak of the axial power profile, and the trapped-stack configuration begins. As the reactor power is increased further, additional axial nodes experience PCMI and the length of the trapped stack reduces. The trapped stresses at the axial nodes that were previously in the trapped stack should be included in the PCMI analyses. The trapped stresses at an axial node will be released when that node is no longer in the trapped-stack configuration and is not experiencing any PCMI.

Figure 2 presents five different states of the trapped-stack configuration. Figure 2(a) shows the beginning of the trapped stack. The lowest elevation of PCMI is the sixth axial node, so the trapped stack consists of five axial nodes. The trapped stresses (stresses due to trapped-stack configuration) in the cladding and pellet column are T_1 (tensile) and C_1 (compressive), respectively. As the reactor power increases further, axial Nodes 4 and 5 experience PCMI and the trapped-stack length reduces and consists of three axial nodes as shown in Figure 2(b). The trapped stresses in the cladding and pellet column of the shortened trapped stack are increased to T_2 (tensile) and C_2 (compressive), respectively. The trapped stresses T_1 and C_1 at axial Nodes 4 and 5 are included in the PCMI analysis.

Figure 2(c), (d), and (e) represent the trapped-stack configurations, while the stack length is increasing. At time t, the PCMI at Node 4 is released, and the trapped-stack length is increased from three axial zones [Figure 2 (b)] to four axial zones as shown in Figure 2(c). At time t when the increase in the trapped-stack length takes place, the axial stresses at the first three nodes are T_2 and C_2 and at Node 4 they are T_1 and C_1. Figure 2(d) represents the trapped-stack configuration at time t after axial equilibrium is satisfied and the trapped stresses at the first four nodes are the same and equal to T_3 and C_3. As the rod power decreases further, the remaining locked nodes are released and the trapped stresses are reduced to zero, Figure 2(e).

2.3 Relocation Model

The fuel relocation model is a function of burnup, power, and initial gap. The correlation developed by Shimade and Oguma [9] is used. Shimade and Oguma found that a reasonable correlation exists between fuel relocation and the number of cracks in a pellet. They also assumed that the dependence of relocation on power and burnup is similar to that of the number of cracks. The number of cracks in a pellet increases rapidly with increasing burnup until about 5.0 MWd/kgUO_2 after which the number of cracks remain constant. Below

5.0 MWd/kgUO_2, the number of cracks in a pellet is directly proportional to power from 10 to 40 kW/m and constant thereafter. The correlation presented in Reference 9 is

$$R_e = G_o[0.4 + (0.01\ P - 0.3)e^{aBu}] + (0.6\ G_o - A)(1 - e^{bBu}). \tag{1}$$

where R_e is relocation (m), G_o is as-fabricated fuel-cladding gap (m), P is linear heat rate (kW/m), BU is burnup (MWs/kgU), and a, b, and A are experimental constants. The empirical constants were determined using experimental data from two Halden tests, IFA-211 and IFA-410. The constants are: $A = 6.5 \times 10^{-5}$, $a = -2.5463 \times 10^{-5}$ and $b = -0.9576 \times 10^{-5}$. This model is used in the FRAP-T6 code to calculate fuel relocation strain until PCMI occurs. The fuel relocation strain is assumed to remain constant during PCMI.

2.4. Effective Fuel Thermal Expansion Model

FRACAS-II performs an axisymmetric analysis to calculate the elastic-plastic-creep response of fuel and cladding subjected to mechanical and thermal loadings. Fuel pellets are assumed to be flat ended and are analyzed assuming generalized plane strain. During axial PCMI, the differential axial thermal expansion of the fuel stack is imposed on the cladding tube resulting in axial elongation of the cladding.

Thermal expansion of the fuel stack depends on rod power, rate of power increase, and the pellet design parameters. The pellet design parameters include the length of pellet and shape of the pellet ends. The pellet ends may be flat or dished, and/or chamfered.

The axial thermal expansion of a fuel stack having pellets with dished ends is less than that having pellets with flat ends [10]. A fuel stack having long, dish-ended pellets will expand more than a stack having short, dish-ended pellets. A model is based on experimental measurements developed to modify the axial thermal expansion of a fuel stack having flat-ended pellets to account for the design parameters. This model defines a design factor based on the pellet design parameters and calculates the effective thermal expansion of fuel by multiplying the design factor with the axial thermal expansion of fuel stack having flat-ended pellets. The design factor for long, flat-ended pellets is equal to 1.0 and for 15-mm long, dish-ended pellets is equal to 0.25.

3. Comparison of Calculations with Test Measurements

The measurements of cladding axial elongation from two experiments, IFA-508 Rod 11 [11] and IE-1 Rod 7 [12], are compared with the corresponding FRAP-T6 calculations. The fuel rods in both experiments have dish-ended, 15.0-mm long pellets. The size of the as-fabricated gap is 0.05 mm for Rod 11 and 0.1149 mm for Rod 7. The axial power profile had a peaking factor of 1.1 for Rod 11 (IFA-508) and 1.72 for Rod 7 (IE-1).

Rod 11 was tested at beginning-of-life, while Rod 7 was tested at 6.8 GWd/mtU burnup. For the FRAP-T6 analyses of Rod 11, experimental measurements of cladding axial elongation and hoop strains are used to determine that the magnitude of the locking gap is equal to 0.02 mm (40% of the as-fabricated cold gap). For Rod 7, the FRAP-T6 calculations of cladding hoop strains and the experimental measurement of cladding axial elongation are used to determine that the magnitude of the locking gap is equal to 0.0 mm. The locking gap magnitude of zero implies that the pellets in Rod 7 had become concentric due to pretest power cycles.

Figure 3 shows a comparison of calculated and measured relative cladding extension for Rod 11 (IFA-508) versus fuel rod peak power. At maximum power, the FRAP-T6 calculation of relative cladding extension is 6% greater than the corresponding measurement. FRAP-T6 calculations showed 0.2 mm relaxation of the cladding axial extension when peak power was held constant at 54 kW/m, while the corresponding measurement is 0.38 mm. Because the axial power profile was quite flat, the axial stresses due to the trapped stack configuration were small (4 MPa).

Figure 4 shows a comparison of calculated and measured relative cladding extension for Rod 7 (IE-1) versus fuel rod average power. At 50 kW/m, the FRAP-T6 calculation of relative cladding extension is 1% greater than the corresponding measurement. FRAP-T6 calculations showed 0.4 mm relaxation of the cladding axial extension when average power was held at ∿50 kW/m, while the corresponding measurement was 0.2 mm. The axial stresses due to the trapped stack configuration were 46.0 MPa (∿25% of the cladding yield strength).

4. Conclusion

The cladding deformation models presented in Section 2 have been tested through comparison with experimental data. Based on the comparisons presented in Section 3, the following conclusions are made:

1. FRAP-T6 accurately calculates the axial elongation of cladding which is needed to determine the uniform axial stress in cladding. Uniform axial stress is one of the three components required to determine cladding failure due to SCC.
2. The calculated thermal expansion of the fuel should be multiplied by the design factor to take into account the pellet design parameters (length of pellet and shape of the pellet ends). FRACAS-II calculates the thermal expansion of the fuel stack assuming that the pellets are flat-ended and in the generalized plane strain condition. The design factor is a constant and depends upon the pellet design parameters.
3. The trapped-stack model is important in calculating the uniform axial stresses in the cladding, provided the axial power profile is not flat. Cladding axial stresses due to trapped-stack configuration were at 25% of the yield strength of the cladding used in the IE-1 Rod 7 experiment.
4. At relatively high burnup, the fuel pellets are concentric and axial and radial PCMI starts at the same power. This conclusion is supported by the use of the locking gap of zero magnitude to analyze the IE-1 Rod 7 at 6.8 GWd/mtU burnup.
5. As the relaxation in cladding extension is due to fuel creep, the discrepancy between the FRAP-T6 calculation and measurement of relaxation may be reduced by replacing the fuel creep model in FRAP-T6 [13] by the MATPRO model FCREEP [14]. The fuel creep model in FRAP-T6 calculates stress as a function of temperature and strain rate, while FCREEP calculates strain rate in fuel as a function of time, temperature, grain size, density, fission rate, oxygen-to-metal ratio, and external stress.

5. References

[1] BERNA, G. A., et al., FRAPCON-2: A Computer Code for the Calculation for Steady State Thermal-Mechanical Behavior of Oxide Fuel Rods, NUREG/CR-1845, December 1980.
[2] SIEFKEN, L. J., et al., FRAP-T6: A Computer Code for the Transient Analysis of Oxide Fuel Rods, EGG-CDAP-5410, April 1981.

[3] BOHN, M. P., FRACAS-II: A Subcode for the Mechanical Analysis of Nuclear Reactor Fuel Rods, CDAP-TR-78-038, September 1978.

[4] HOOPE, N., "Improvements to COMETHE III-J Fuel Rod Modeling Code," Fuel Element Performance Computer Modeling Conference, Blackpool, U.K., March 1978.

[5] WIESENACK, W., "Analysis of Early Axial Interaction with the Fuel Modeling Program MARS," OCED Halder Reactor Project, HWR-327.

[6] SHAH, V. N., CARLSON, E. R., BERNA, G. A., Advanced Deformation Models for FRAP-T6, EGG-CDD-6054, September 1982.

[7] MENDELSON, A., Plasticity: Theory and Application, MacMillan, 1968, pp. 204-208.

[8] BOHN, M. P., FRACAS--A Subcode for the Analysis of Fuel Pellet-Cladding Mechanical Interaction, TREE-NUREG-1028, April 1977, pp. 38-41.

[9] SHIMADE, S., and OGUMA, M., "Analysis of Fuel Relocation Using In-Pile Data from IFA-211 and IFA-410," Enlarged Halden Programme Group Meeting on Fuel Performance Experiments and Evaluation, Volume III, HPR-229, August 1979.

[10] AAS, A., "Mechanical Interactions Between Fuel and Cladding," Nuclear Engineering and Design, 21, 1972, pp. 237-253.

[11] UCHIDA, M., and ICHIKAWA, M., "In-Pile Diameter Measurement of Light Water Reactor Test Fuel Rods for Assessment of Pellet-Cladding Mechanical Interaction," Nuclear Technology, November 1980, pp. 33-44.

[12] QUAPP, W. J., et al., "Irradiation Effects Test Series Test IE-1," Test Results Report, TREE-NUREG-1046, March 1977.

[13] BOHABOY, P. E., ASAMOTO, R. R., and CONTI, A. E., Compressive Creep Characteristics of Stoichiometric Uranium Dioxide, GEAP-10054, May 1969.

[14] HAGRMAN, D. L. (ed.), MATPRO Version 11 (Revision 1): A Handbook of Materials Properties for Use in the Analysis of Light Water Reactor Fuel Rod Behavior, NUREG/CR-0497, TREE-1280, Rev. 1, February 1980, pp. 64-83.

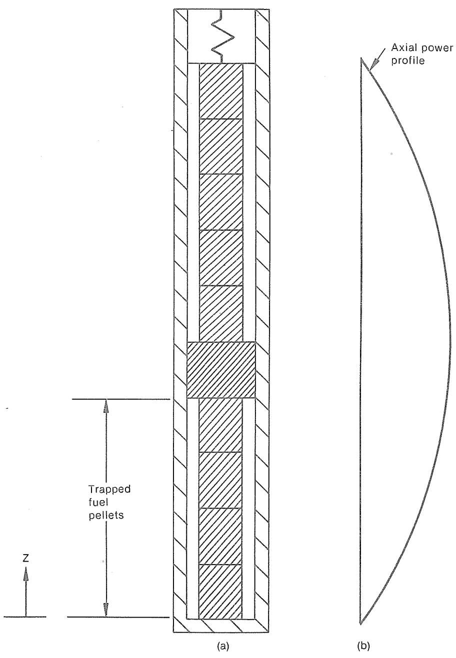

Figure 1. Trapped-stack configuration.

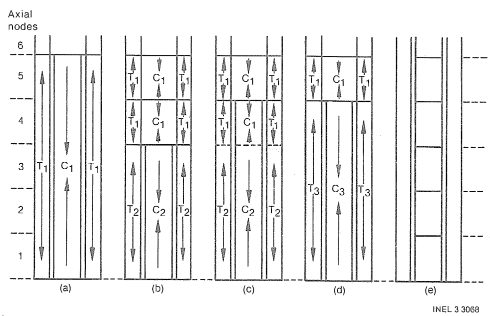

Figure 2. Five different states of trapped-stack configurations: (a) initiation of trapped-stack conditon, (b) shortened trapped stack, (c) extended trapped stack - before equilibrium is satisfied, (d) extended trapped stack - after equilibrium is satisfied, and (e) trapped-stack condition is released.

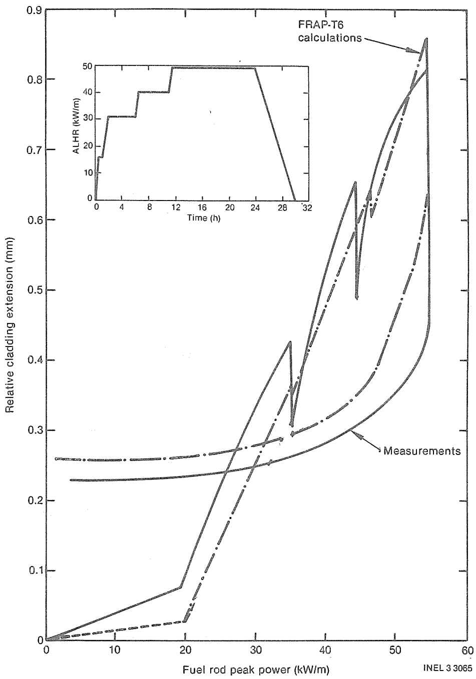

Figure 3. Calculated and measured cladding axial extension versus power for IFA-508 Rod 11.

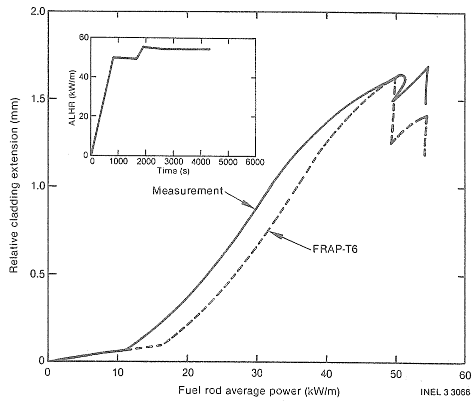

Figure 4. Calculated and measured cladding extension versus power for IE-1 Rod 7.